Study of the scavenging behavior and structural changes accompanying the interaction of aqueous Pb2+ and Sr2+ ions with calcite

3 authors, including:

Talal Shahwan
Birzeit University
54 PUBLICATIONS **1,293** CITATIONS

Study of the scavenging behavior and structural changes accompanying the interaction of aqueous Pb²⁺ and Sr²⁺ ions with calcite

T. SHAHWAN,* B. ZUNBUL and D. AKAR

Department of Chemistry, Izmir Institute of Technology, 35430 Urla, Izmir, Turkey

The uptake of Pb²⁺ and Sr²⁺ ions from aqueous solutions by calcite was studied at various initial concentrations and pH conditions using the batch method under ambient conditions. XRPD, SEM/EDS, AAS/AES, and DRIFT techniques were used in characterizing the sorption process. The results indicated that the retention mechanism of Pb²⁺ and Sr²⁺ ions ranged from ion incorporation to precipitate overgrowth (cerussite, hydrocerussite for Pb, strontianite for Sr) depending on the concentration and pH conditions. The calcite structure seemed to be entirely vanishing upon formation of cerussite and hydrocerussite while partial dissolution of calcite occurred upon strontianite formation. The formation of precipitates showed rapid kinetics, and equilibrium seemed to be reached within about an hour from the start of mixing. SEM analysis showed that cerussite, hydrocerussite, and strontianite had columnar prismatic-like, tabular hexagonal-like, and needle-like morphologies. Based on a nine-month observation period, dry samples of hydrocerussite seemed to show more morphological stability than cerussite. EDS analysis indicated that Pb²⁺ sorption is more favored than that of Sr²⁺, particularly in the phase of precipitate overgrowth. DRIFT analysis indicated a change in the symmetry of the carbonate groups in calcite matrix upon uptake of Pb²⁺ and Sr²⁺ cations.

Keywords: calcite, Pb²⁺, Sr²⁺, strontianite, cerussite, hydrocerussite

INTRODUCTION

Lead is an element that is continuously discharged into the biological environment as a result of various individual and industrial activities (gasoline, batteries, paints, insecticides, pipes, etc.). Due to its potential threat to the living system, Pb is classified at the top of the priority list of the most hazardous substances along with As, Hg, C_2H_3Cl, and C_6H_6 (Godelitsas *et al.*, 2003).

Strontium is an element that possesses radioactive isotopes like ^{89}Sr ($t_{1/2} = 50.5$ d) and ^{90}Sr ($t_{1/2} = 28.5$ y), which are produced in high rates during the fission reactions and considered among the most important radionuclides from radioactive waste point of view (Lieser, 1995).

Due to their potential detriment towards the living systems, the sorption behavior of both elements on various types of soil fractions has been widely investigated (ex., Hooda and Alloway, 1998; Ponizovsky and Tsadilas, 2003; Adhikari and Singh, 2003; O'Reilly and Hochella, 2003; Abollino *et al.*, 2003; Axe *et al.*, 2000; Sahai *et al.*, 2000; Cherniak, 1997).

The large availability of carbonate minerals in the earth crust makes them among the most important minerals that are responsible for dispersion/accumulation behavior of various metals and hence affecting the biogeochemical cycles of these metals in the environment. These minerals play a major rule in the chemical regulation of aquatic environments via precipitation, dissolution, and sorption reactions which are in turn controlled by the chemical processes taking place at the interface between the mineral lattice and the bulk solution (Morse, 1986).

$CaCO_3$ can exist in three polymorphs; calcite, aragonite, and vaterite. Among these three polymorphs, calcite is the most thermodynamically stable one at room temperature and atmospheric pressure. Calcite possesses a rhombohedral/hexagonal structure with the trigonal carbonate ions being coplanar. The planes containing carbonate ions are perpendicular to the c-axis and they are rotated by 60° from one carbonate layer to the next (Kuriyavar *et al.*, 2000).

Knowledge of the nature of interaction of the metal ions with carbonate minerals is essential in predicting the extent to which they could be fated by these ions, the thing leading to retarding their dispersion into the environment. Recently, the increased applications of various surface-sensitive spectroscopic and microscopic techniques in sorption studies is enabling an understanding of this process on molecular-level the thing providing a better understanding of the mechanisms of interactions between different ions and sorbents. A limited number of such studies were devoted to characterizing the interac-

*Corresponding author (e-mail: talalshahwan@iyte.edu.tr)

tion of Pb^{2+} and Sr^{2+} ions with calcite (e.g., Pingitore *et al.*, 1992; Parkman *et al.*, 1998; Godelitsas *et al.*, 2003; Hay *et al.*, 2003).

In this study, the scavenging of Pb^{2+} and Sr^{2+} ions by calcite at different loadings was investigated. The experiments were performed under ambient CO_2 pressure. One duplicate set of the mixtures was allowed to react in an uncontrolled pH medium. In the second set of mixtures the initial pH was increased to 10.0 units. X-ray Powder Diffraction (XRPD) was used to reveal the change in the calcite structure and detect the possible precipitate formations following sorption. The morphology and the elemental composition of calcite surface before and after sorption was analyzed using Scanning Electron Microscope/Energy Dispersive X-ray Spectroscopy (SEM/EDS). The bulk concentration of Ca^{2+}, Sr^{2+}, and Pb^{2+} ions was measured using Atomic Absorption/Emission Spectroscopy (AAS/AES). Diffuse-Reflectance Infrared Spectroscopy (DRIFT) was applied to analyze the vibrational modes of carbonate specie before and after sorption.

EXPERIMENTAL

All the experiments were carried out using the batch method. Aqueous solutions of $Pb(NO_3)_2$ and $Sr(NO_3)_2$ were prepared using distilled water at concentrations of 1.0×10^{-1}, 1.0×10^{-3}, 1.0×10^{-5} M (mol/l). 100.0 ml aliquots of solutions were added to 1.0 g powder samples of calcite ($CaCO_3$; Carloerba), and mixed in 250 ml Erlenmeyer flasks using magnetic stirrers. The powders were used as received from the manufacturer and size fractionation by dry sieving indicated a wide distribution ranging from 48 μm to 600 μm. Mixing was performed under ambient pressure and temperature conditions for time periods ranging from 10 minutes up to four hours.

The experiments were carried in two sets, one of them with no pH control and the second with the initial pH raised to a value of 10.0 units using a 0.010 M solution of NaOH. The pH variations are reported and discussed in the part of "results and discussions" that follows. At the end of the mixing period, the solid phases were separated from the solution by filtration and dried at 50°C for 24 hours. The liquid concentrations of Pb, Sr, and Ca were determined using AAS/AES measurements, which were conducted using a Thermal Elemental SOLAAR M6 Series-type instrument. Pb and Sr were analyzed in AAS mode with hollow cathode lamps (λ(Pb) = 217.0 nm, λ(Sr) = 460.7 nm) applied as light sources. The analysis of Ca was performed using AES at λ = 422.7 nm. During analysis, air was used as an oxidant, and acetylene as a fuel.

The solid samples were analyzed using XRPD, SEM/EDS, and DRIFT. The XRPD analysis was performed using a Philips X'Pert Pro diffractometer. The samples

were first ground, mounted on holders then introduced for analysis. The source consisted of Cu K_{α} radiation (λ =1.54 Å). Each sample was scanned within the 2 theta range of 15–60. The step size was 0.020 with a time per step duration of 0.6 s.

SEM/EDS characterization was carried out using a Philips XL-30S FEG type instrument Prior to analysis, the solid samples were sprinkled onto adhesive aluminum tapes supported on metallic disks and then coated using deposited Au-Pd vapor. Images of the sample surfaces were then recorded at different magnifications. Elemental analysis was performed at four different points randomly selected on the solid surface and the average of the results was reported.

DRIFT technique was used to collect the spectra of the samples in the middle IR region using a Nicole Magna 550 type instrument. The samples were introduced as powders mixed with KBr and the spectra were recorded in the range 400–4000 cm^{-1}. The KBr powder was used as a background. A total of 32 scans were recorded with a resolution of 4 cm^{-1} for each spectrum. Omnic 1.3 software was used to process the results.

RESULTS AND DISCUSSION

The XRPD analysis indicated that the $CaCO_3$ fractions used in this study were entirely composed of calcite polymorph. The sample is characterized by the major features occurring at d_{104} = 3.069 Å, d_{110} = 2.488 Å, d_{113} = 2.288 Å, d_{202} = 2.092 Å, d_{018} = 1.949 Å, d_{116} = 1.892 Å. This was verified also by the DRIFT analysis which showed the presence of the characteristic bands of calcite. In general, the vibrational spectra of carbonate minerals contain modes arising from the symmetric stretching mode (ν1), out-of-plane bending (ν2), the asymmetric stretching (ν3), the in-plane-bending (ν4), in addition to the two combination modes (ν1 + ν3) and (ν1 + ν4) (Böttcher *et al.*, 1997). Based on this, the bands at 712, 878, 1437, 1789, and 2509 in the DRIFT spectrum of pure calcite were assigned to the vibrational modes ν4, ν2, ν3, ν1 + ν3, and ν1 + ν4, respectively. The band corresponding to the vibrational mode ν1 was absent. In calcite, the carbonate ion has a D_{3h} point group (Reig *et al.*, 2002), for which the symmetric stretching mode (ν1) is IR inactive.

The calcite samples were also characterized using SEM. The micrographs obtained at ×15000 and ×50000 magnifications showed that the mineral is composed of aggregates of various sizes. The EDS results showed that the mineral consists of C, O, and Ca with atomic percentages of 36.9 ± 6.9, 47.3 ± 3.2, and 15.8 ± 3.7, respectively. These numbers corresponds to arithmetic averages of the data taken from four different locations. The reported errors correspond to the standard deviations in the data. Adventitious O and/or C—those arising from sources

Table 1. The bulk concentration of Ca following the sorption experiments of Pb and Sr on calcite obtained using AAS/AES

Initial conc. (M)	Ca concentration (ppm)			
	Pb^{2+} sorption experiments		Sr^{2+} sorption experiments	
	Set 1	Set 2	Set 1	Set 2
1.0×10^{-5}	15	21	<1	<1
1.0×10^{-3}	32	34	22	27
1.0×10^{-1}	1681	1521	851	917

other than the analyzed sample—might frequently cause anomalies in the measured data.

Analysis of the samples prepared in uncontrolled pH medium

In these experiments, no pH adjustment was attempted and all the mixtures were reacted under atmospheric CO_2 pressure. The pH measurements performed once every 15 minutes during the calcite-solution contact period showed that the pH changed within the ranges 9.1–8.5, 8.7–8.4, and 7.6–7.3 for solutions with initial Pb^{2+} concentration of 1.0×10^{-5}, 1.0×10^{-3}, and 1.0×10^{-1} M, respectively. On the other hand, in the case of Sr^{2+} uptake, the pH ranged within 9.0–8.2, 8.9–8.2, and 7.7–7.5 for the initial concentrations of 1.0×10^{-5}, 1.0×10^{-3}, and 1.0×10^{-1} M, respectively. It is well known that in aqueous media, carbonate (CO_3^{2-}) ions dominates if the pH is larger than pKa_2 of carbonic acid (=10.3). In the pH range 6.4–10.3, the dominating specie will be HCO_3^-, and if the pH goes below pKa_1 (=6.4), then carbonic acid starts to form. Hence, it is evident from the pH data that increasing the initial concentration of Pb^{2+} and Sr^{2+} ions enhanced the acidity of the medium, thus contributing to an increased surface dissolution of calcite and as a result release of more CO_3^{2-} and Ca^{2+} ions. This enhanced dissolution was verified using the data obtained from AES measurements performed to measure the Ca concentration in the bulk solutions at the end of the sorption experiments. The results of those measurements are given in Table 1. The data indicates a large jump in the concentration of released Ca upon increasing the initial concentration of Pb^{2+} and Sr^{2+} ions to 0.10 M. The large depletion of Ca^{2+} resulting from the intense dissolution of calcite matrix indicates a parallel increase in the CO_3^{2-} concentration available in the bulk of solution.

The XRPD characterization of Pb-, and Sr-reacted calcite samples (Figs. 1(a) and (b)) showed that while only some slight intensity reductions were observed in the calcite peaks at 1.0×10^{-5}, and 1.0×10^{-3} M initial concentrations of the sorbed ions, formation of cerussite (PbCO$_3$) and strontianite (SrCO$_3$) occurred as the initial concen-
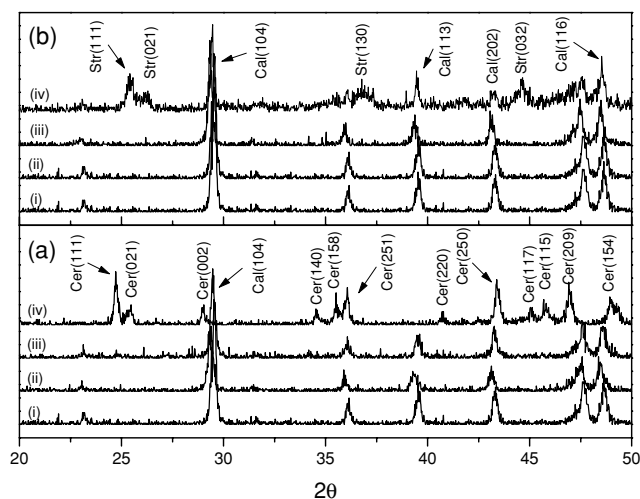

Fig. 1. XRPD diagrams of: (a) Pb-sorbed calcite, (b) Sr-sorbed calcite (i) pure calcite, (ii) initial concentration = 1.0×10^{-5} M, (iii) initial concentration = 1.0×10^{-3} M, (iv) initial concentration = 1.0×10^{-1} M, Cer: cerussite, Str: strontianite.

tration of Pb^{2+} and Sr^{2+} was raised to 0.10 M. Furthermore, Fig. 1(a) suggests that the features of calcite disappeared almost totally upon cerussite formation. On the other hand, strontianite formation is seen to be accompanied by partial intensity reductions of the calcite peaks, as given in Fig. 1(b), indicating a partial dissolution of the mineral in this case.

The crystal overgrowth of cerussite and strontianite was studied also as a function of time. Calcite samples were reacted with Pb^{2+} and Sr^{2+} solutions with initial concentration of 0.10 M at mixing periods of 10 minutes, 30 minutes, 1 hour, 2 hours, and 4 hours. The XRPD characterization of the samples indicated fast overgrowth of cerussite and strontianite; within 10 minutes after the start of mixing as shown in Figs. 2(a) and (b) for the sorption of Pb^{2+} and Sr^{2+}, respectively. Moreover, the figures reveal a faster dissolution of calcite when contacted with Pb^{2+} ions and a complete disappearance of calcite features by the end of about one hour of mixing. The partial
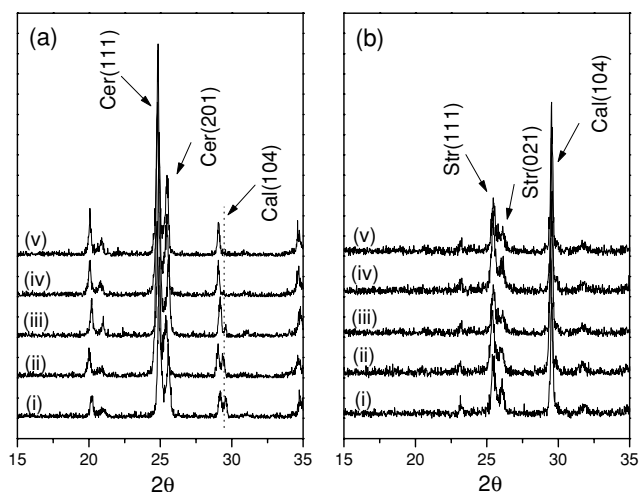
Fig. 2. XRPD diagrams showing the overgrowth of cerussite (a), and strontianite (b) as a function of mixing time. (i) 10 minutes, (ii) 30 minutes, (iii) 1 hour, (iv) 2 hours, (v) 4 hours.

Fig. 3. SEM micrographs of: (a) cerussite (magnification of ×50,000), (b) strontianite (magnification of ×100,000).

dissolution of calcite, in the case of Sr^{2+} uptake, seems to cease in less than a ten-minute period after the start of mixing. The termination of dissolution is paralleled with an "apparent" achievement of saturation in the overgrowth of cerussite and strontianite as indicated by the peak intensities. This is indicative that simultaneous dissolution/crystal overgrowth processes are taking place upon the sorption of both of Pb^{2+} and Sr^{2+} ions. Similar observations were reported for Pb^{2+} uptake on calcite and aragonite polymorphs (Godelitsas et al., 2003).

Formation of cerussite and strontianite was also verified using SEM analysis as shown in Fig. 3. In line with the XRPD predictions, SEM micro-images demonstrated no distinguishable change in the calcite surface for the mineral samples prepared with initial Pb^{2+} and Sr^{2+} concentrations of 1.0×10^{-5} and 1.0×10^{-3} M. As the initial concentration of both cations was raised to 0.10 M, a massive overgrowth of cerussite and strontianite was observed. Figure 3(a) shows that the cerussite crystals possess a columnar prismatic morphology. Strontianite crystals, however, assumes a needle-like morphology as demonstrated by Fig. 3(b).

EDS analysis was carried out to determine the atomic percentages of Pb^{2+} and Sr^{2+} ions in the carbonate matrices following the uptake processes. The EDS results, which are given in Table 2, correspond to findings obtained for duplicate sets of experiments at different initial metal concentrations. The table contains also the atomic percentages of Ca^{2+} obtained from the same samples. Each of the results represents an average of four EDS measurements taken at various locations on the solid surface and the reported errors refer to the standard deviation in these results. The increased depletion in Ca
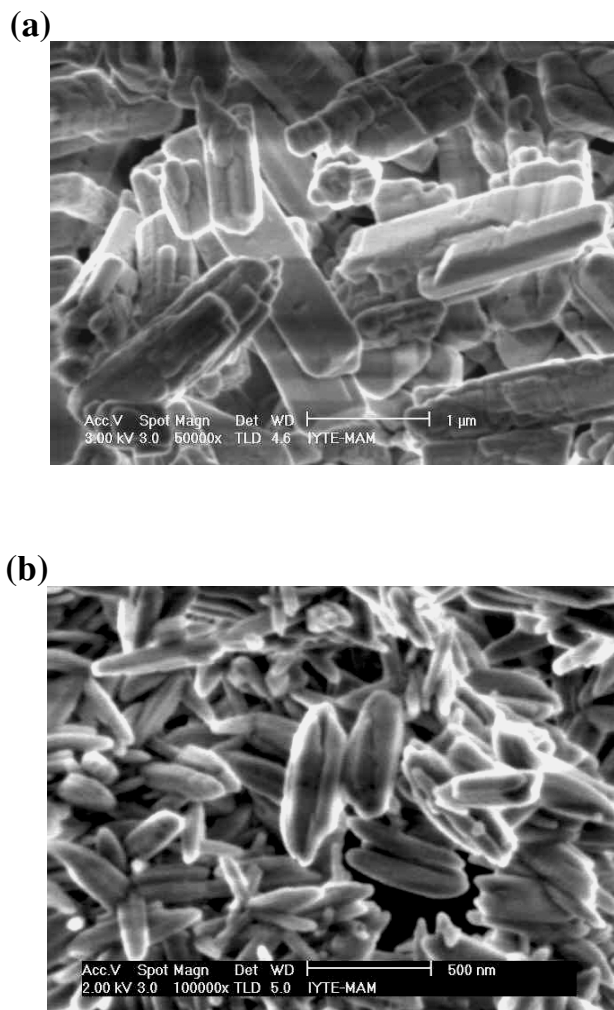
content verifies the AES results, the thing referred to the enhancement in calcite dissolution upon increasing the initial concentration of Pb^{2+} and Sr^{2+}. The data shows clearly that Pb^{2+} uptake is more favored than that of Sr^{2+} at all initial concentrations. Upon overgrowth of cerussite and strontianite, a large increase in the sorbed amounts of Pb^{2+} and Sr^{2+} is observed in parallel with a larger gap between the scavenged quantity of each of these ions.

In literature, it is stated that, at low initial metal concentrations, the uptake mechanism by carbonates is due to an initial fast adsorption reaction followed by a slower step of fixation of ions onto the carbonate surface, while at higher metal concentrations surface precipitation occurs leading to formation of carbonate and hydroxycarbonate as discrete phases (Schosseler et al., 1999). Reported investigations of the sorption behavior of calcite towards Sr^{2+} ions indicated that the type of up-

Table 2. EDS results giving the atomic percentages of Pb and Sr in the carbonate matrice obtained from duplicate sets of experiments at different initial concentrations

Initial conc. (M)	Experimental set	Pb-sorbed calcite		Sr-sorbed calcite	
		Ca	Pb	Ca	Sr
1.0×10^{-5}	1	15.7 ± 1.3	0.1 ± 0.0	14.5 ± 2.6	N.D.
	2	19.7 ± 3.7	0.1 ± 0.0	15.1 ± 1.9	N.D.
1.0×10^{-3}	1	11.3 ± 2.2	2.7 ± 0.6	14.6 ± 3.4	0.2 ± 0.1
	2	15.2 ± 1.8	1.2 ± 0.9	14.9 ± 0.7	0.2 ± 0.1
1.0×10^{-1}	1	2.2 ± 1.2	8.6 ± 3.8	5.9 ± 2.1	2.3 ± 0.3
	2	1.5 ± 0.5	12.3 ± 0.6	6.2 ± 1.3	1.7 ± 0.2

N.D.: Not Detected.

Table 3. The ionic radii of Ca^{2+}, Sr^{2+}, and Pb^{2+} and Gibbs free energies of formation of the aqueous cations. The table provides also the calculated log $D_{Me,ideal}$ which shows the theoretical partitioning at the calcite/ solution interface.

Cation	Radius (Å)	$\Delta G^{o}_{f,cation}$ (kcal/mol)	$\Delta G^{o}_{f,MeCO3}$ (kcal/mol)	$logD_{Me,ideal}$
Ca^{2+}	1	−132.12	−270.0	—
Sr^{2+}	1.16	−133.72	−270.3	−0.9
Pb^{2+}	1.18	−5.79	−146.0	1.8

take mechanism is closely related to the coordination number of the sorbed ion in its structural environment (Parkman *et al.*, 1998). At low Sr^{2+} loadings, measurements of the Sr-O bond length was found to correspond to an approximately six-fold coordination, resembling the hexagonal (rhombohedral) structural environment of calcite. At high Sr^{2+} loadings, however, the Sr-O bond length seems to be close to a nine-fold coordination as it is the case in the orthorhombic strontianite (Parkman *et al.*, 1998; Pingitore *et al.*, 1992). A six-fold coordination of Pb on calcite was also documented. In a study using Synchrotron X-ray standing wave and X-ray reflectivity, it was reported that most of the sorbed Pb^{2+} ions (conc. 2– 25 ppm) by calcite surface occupy Ca^{2+} sites (Sturchio *et al.*, 1997). Furthermore, the differences between the sorbed amounts of both cations might be referred to different types of incorporation mechanisms. It is reported that, at low concentrations (10^{-8} to 10^{-4} M), the ionic radii of the divalent cations determines the extent of uptake of these cations by calcite so that ions with smaller radii are more preferably sorbed (Zachara *et al.*, 1991). Although the ionic radii criterion proved to be successful in explaining the preferential sorption of various ions on calcite (Zachara *et al.*, 1991; Curti, 1999), it can not be used to explain the higher selectivity of calcite towards Pb^{2+} ions over that of Sr^{2+} ions since both of them possess identical charges and close ionic radii as given in Table 3. Similar deviations of the ionic radii criteria were

observed also for pairs of cations possessing similar ionic radii like Zn^{2+} and Mg^{2+}, Na^+ and La^{3+} ions (Curti, 1999). The explanation offered for such anomalies relied on the hypothesis suggesting that ions with lower partition coefficients are trapped within the limited number of interstitial positions in calcite rather than exchanging with Ca^{2+} in lattice positions (Busenberg and Plummer, 1985). The larger partition coefficient for Pb^{2+} can be verified from a thermodynamic approach which covers the possibility that both of Pb^{2+} and Sr^{2+} ions might be incorporated within orthorhombic positions of calcite (Böttcher, 1997). According to this approach, the partition coefficients are calculated as:

$$logD_{Me,ideal} = (\Delta G^{o}_{f,CaCO3(s)} - \Delta G^{o}_{f,MeCO3(s)} - \Delta G^{o}_{f,Ca2+(aq)} + \Delta G^{o}_{f,Me2+(aq)})/((\ln(10))RT).$$

Where ΔG^{o}_{f} correspond to the standard Gibbs free energies of formation for the rhombohedral solid carbonates and the aqueous cations, T is the temperature in K, and R is the gas constant (1.98717 cal/mol.K). The equation above may serve as a first aid for the evaluation of the degree of solid-solution formation with calcite of trace metals which do not form otherwise stable end member carbonates with the $R\bar{3}c$ space group (Böttcher, 1997). Based on the equation above and the corresponding values of ΔG^{o}_{f} (Sverjensky and Molling, 1992) given in Table 3, it is possible to calculate log $D_{Me,ideal}$ of Sr^{2+} and

Pb^{2+} as –0.9 and 1.8 which correspond to partition coefficients of 0.13 and 63, respectively. This approach is useful in particular at lower metal concentrations where the possibility of incorporation of the sorbed metal ions by the rhombohedral calcite sites is higher.

At high loadings, the extent of precipitate overgrowth of a given cation can be related with the K_{sp} of the cation-anion pair forming the precipitate. Theoretically, in a mixture where the reactants are highly dispersed, the extent to which cation species reacts with calcite can be estimated using the individual K_{sp} values (Hay $et\ al.$, 2003):

$$CaCO_3 + Me^{2+} \rightarrow Ca^{2+} + Me^{2+} + CO_3^{2-} \rightarrow MeCO_3 + Ca^{2+},$$
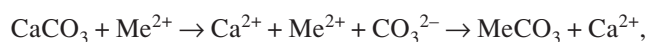
where Me^{2+} stands for a divalent metal ion. The net solubility product is then:

$$K_{CaCO_3 \rightarrow MeCO_3} = \frac{K_{sp,CaCO_3}}{K_{sp,MeCO_3}} = \frac{\left[Ca^{2+}\right]}{\left[Me^{2+}\right]}.$$

Utilizing the K_{sp} values of 4.5×10^{-9}, 7.4×10^{-14}, and 9.3×10^{-10} for CaCO$_3$ (calcite polymorph), PbCO$_3$, and SrCO$_3$, respectively (Skoog $et\ al.$, 1996), the net solubility products are calculated to be ~61 000 and ~5 for cerussite and strontianite formation respectively. These results are indicative that while the reaction between Sr^{2+} and CO$_3^{2-}$ would be—to a certain extent—driven towards strontianite formation, the reaction of Pb^{2+} with CO$_3^{2-}$ would proceed until almost all calcite is converted into cerussite. These predictions are supported also by Fajans' coprecipitation rule used for qualitative predictions of the extent of precipitate formation of radioelements with counter ions (Curti, 1999). According to this law; "the lower the solubility of the compound formed by the radioelement with the anion of the precipitate, the greater is the amount of the radioelement carried down as cation". It is obvious that these predictions qualitatively explain the larger removal of Pb^{2+} ions (in the form of cerussite) compared to the removal of Sr^{2+} (via strontianite overgrowth) at higher loadings of these ions on calcite. However, it must be noted that the above discussion is based solely on a thermodynamic approach, and thus careful comparison between experimental and these theoretical predictions should be done, as such models usually lack a kinetic perspective.

The effect of Pb^{2+} and Sr^{2+} uptake on the symmetry of carbonate groups was studied using DRIFT. In general, FTIR spectroscopy is considered as a useful tool in the molecular characterization of inorganic species and has certain advantages over other techniques, namely the requirement of only a small quantity of the analyzed sample, quick and easy sample preparation and short analy-
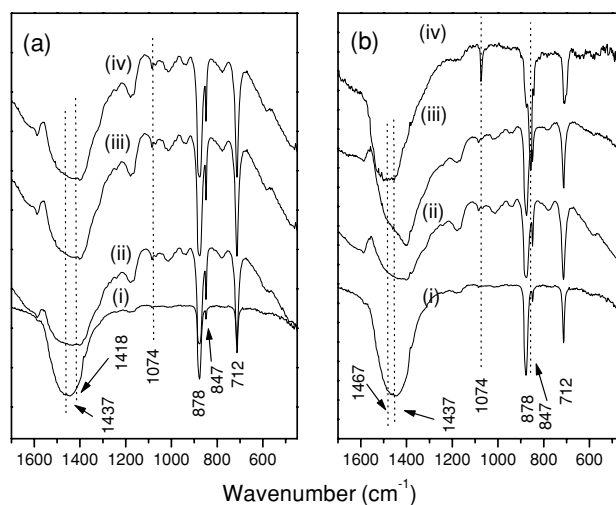

Fig. 4. DRIFT spectra of : (a) Pb-sorbed calcite, (b) Sr-sorbed calcite (i) pure calcite, (ii) initial concentration = 1.0×10^{-5} M, (iii) initial concentration = 1.0×10^{-3} M, (iv) initial concentration = 1.0×10^{-1} M.

sis time. The application of the technique might, however, be complicated due to the appearance of water bands and the wide absorption bands and irregular profiles which make the assignation and identification of the cation-anion pair more complex (Reig $et\ al.$, 2002).

Theoretically, a gaseous carbonate ion is known to possess a trigonal planar shape with a point group of D$_{3h}$. This molecule possesses, as was previously stated, four first order internal modes; $v1$, $v2$, $v3$, and $v4$ with the last two modes being doubly degenerate adding up to a total of six normal modes. Due to symmetry considerations, the selection rules predict that the $v1$ mode is IR inactive. Because of the intermolecular interactions, the symmetry of carbonate ion might be lowered in a crystalline state and the selection rules might consequently be affected, the thing leading to activating initially inactive bands and splitting the degenerate vibrations. When considering molecular vibrations in crystalline states, rather than the isolated gaseous states, the concept of site symmetry is used to predict the plausible changes in the vibrational modes. The site symmetry concept refers to the local symmetry around the center of gravity of a molecule in a unit cell. This approach explains why, for example, calcite and aragonite have different vibrational spectra in spite of the fact that they have the same chemical composition. It can be theoretically shown that the D$_{3h}$ symmetry of carbonate ion is lowered to D$_3$ in the case of calcite and C$_s$ in the case of aragonite the thing that leaves the carbonate vibrational modes unchanged in the case of calcite but activates the $v1$ mode and causes the $v3$ and $v4$ modes to split in the case of aragonite (Nakamoto, 1986). Experimental observations are in
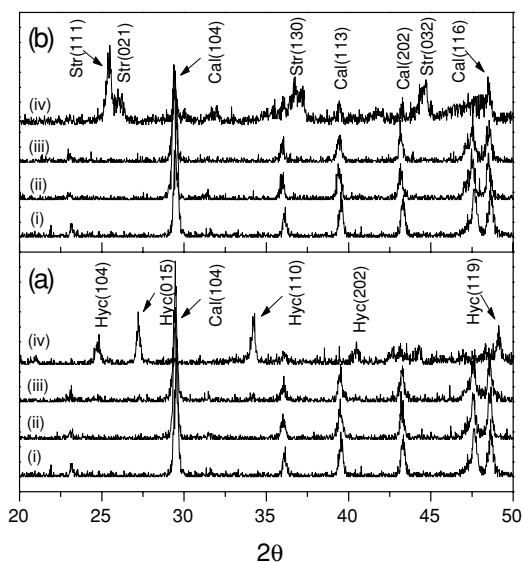
Fig. 5. XRPD diagrams of: (a) Pb-sorbed calcite, (b) Sr-sorbed calcite, (initial pH was raised to 10.0 in all experiments). (i) pure calcite, (ii) initial concentration = 1.0×10^{-5} M, (iii) initial concentration = 1.0×10^{-3} M, (iv) initial concentration = 1.0×10^{-1} M, Hyc: hydrocerussite, Str: strontianote.

Fig. 6. SEM micrographs of: (a) hydrocerussite (magnification of ×50,000), (b) cerussite powder stored under ambient conditions for nine months (magnification of ×25,000).

agreement with these predictions (Kuriyavar *et al*., 2000).

In light of the above information, DRIFT technique was applied to study the effect of possible geometry changes following the uptake of Pb and Sr on the vibrational bands of calcite and elucidate the vibrational bands of other ion carbonates formed as coprecipitates. The basic IR modes of pure calcite are compared with those of Pb- and Sr-loaded calcite in Figs. 4(a) and (b), respectively. The feature appearing near 1074 cm^{-1} in the spectra of both of Pb- and Sr-loaded calcite belongs to the ν1 vibrational mode (symmetric stretching) that is IR inactive in the spectrum of pure calcite. The peak becomes much distinct in the case of strontianite compared to cerussite. Moreover, a broadening is observed in the asymmetric stretching peak (ν3)—which occurred at 1437 cm^{-1} in calcite—accompanied by a blue shift in this mode to about 1467 cm^{-1} upon strontianite formation. Furthermore, the originally weak feature, appearing near 847 cm^{-1} in calcite, is becoming more intense upon sorption of Pb^{2+} and Sr^{2+} ions. It is clear from that the increase in intensity of this band is associated with a decrease in the intensity of the ν2 (out-of-plane bending) mode, the thing mostly pronounced upon strontianite formation.

Analysis of the samples prepared at an initial pH 10.0

These experiments were conducted with the initial pH adjusted to 10.0. Again, pH measurements performed once every 15 minutes during the calcite-solution contact period showed that the pH ranged between 10.0–8.3, 10.0–
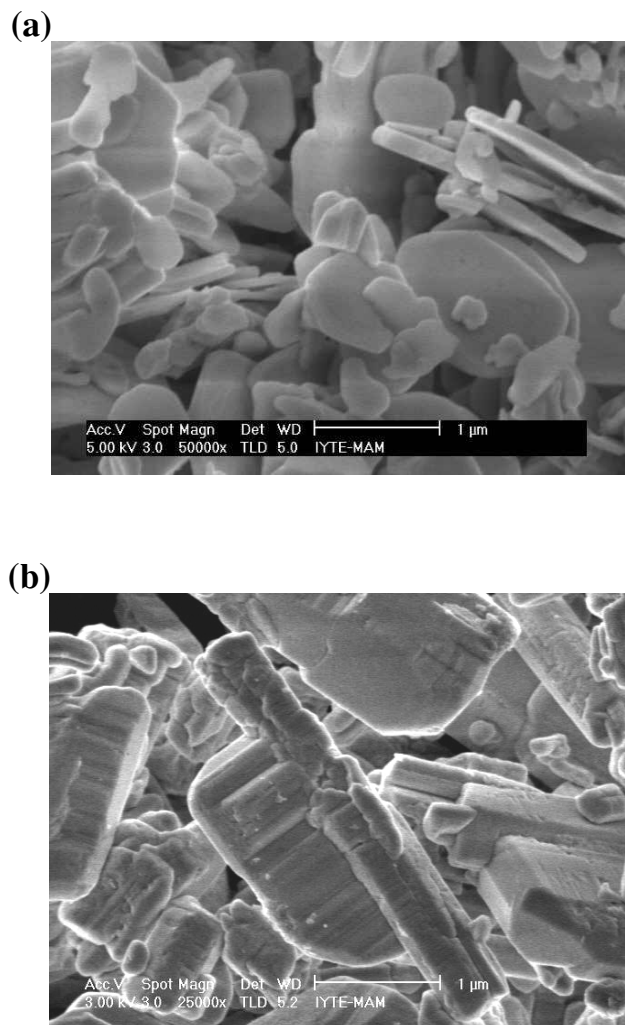
8.4, and 10.0–7.9 for solutions with initial Pb^{2+} concentration of 1.0×10^{-5}, 1.0×10^{-3}, and 1.0×10^{-1} M, respectively. On the other hand, in the experiments of Sr^{2+} uptake, the pH ranged within 10.0–8.2, 10.0–8.2, and 10.0–7.4 for the initial concentrations of 1.0×10^{-5}, 1.0×10^{-3}, and 1.0×10^{-1} M, respectively.

The XRPD patterns of Pb-, and Sr-sorbed calcite are shown in Figs. 5(a) and (b). Like in the first part, the overgrowth of strontianite was observed only when the initial concentration of Sr^{2+} was raised to 0.10 M as revealed by Fig. 5(b). Comparing this figure with Fig. 1(b), it can be seen that the intensity of strontianite reflections upon increasing the initial pH to 10.0 is larger indicating enhancement in the overgrown amount of strontianite. Comparing the calcite reflections in the same figures reveals a further loss in their intensity with the increase in

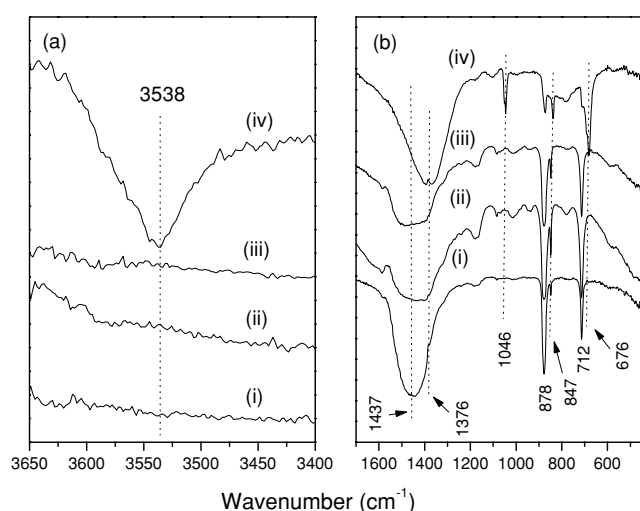| Initial conc. (M)	Experimental set	Pb-sorbed calcite		Sr-sorbed calcite	
		Ca	Pb	Ca	Sr
1.0×10^{-5}	1	16.3 ± 1.7	0.1 ± 0.0	17.7 ± 2.3	0.1 ± 0.0
	2	16.9 ± 0.6	0.1 ± 0.0	16.4 ± 1.2	0.1 ± 0.0
1.0×10^{-3}	1	16.3 ± 1.1	3.1 ± 1.2	17.1 ± 1.0	0.2 ± 0.0
	2	13.5 ± 1.8	2.2 ± 0.7	16.8 ± 1.1	0.2 ± 0.1
1.0×10^{-1}	1	0.9 ± 0.2	30.8 ± 5.0	3.7 ± 0.4	6.8 ± 0.8
	2	1.5 ± 0.3	25.3 ± 4.3	7.9 ± 0.5	7.0 ± 0.2

Fig. 7. DRIFT spectra of : (a) Pb-sorbed calcite, (b) Sr-sorbed calcite, (initial pH was raised to 10.0 in all experiments). (i) pure calcite, (ii) initial concentration = 1.0 × 10⁻⁵ M, (iii) initial concentration = 1.0 × 10⁻³ M, (iv) initial concentration = 1.0 × 10⁻¹ M.

intensity of formed strontianite features. Figure 5(a) indicates that in the case of Pb^{2+}, however, increasing the initial concentration to 0.10 M have caused the formation of hydrocerussite $(Pb_3(CO_3)_2(OH)_2)$—rather than cerussite—associated again with a total loss of calcite features from the figure. SEM characterization showed that strontianite retained the needle-like morphology and that hydrocerussite is of a tabular hexagonal-like shape (the edges look not very sharp) as shown in Fig. 6(a). The formation of hydrocerussite upon uptake of Pb by calcite was reported also by other studies (Marani *et al*., 1995; Lin *et al*., 1995; Godelitsas *et al*., 2003). In these studies, formation of a mixture of cerussite and hydrocerussite was reported. In our case, both the XRPD and SEM characterization did not reveal any cerussite formation accompanying the overgrowth of

hydrocerussite. Literature resources show a disagreement among researchers about the relative stability of cerussite and hydrocerussite, the thing that is referred to the fact that the reaction $3PbCO_{3(s)} + H_2O \Leftrightarrow Pb(OH)_2 \cdot (PbCO_3)_{2(s)} + CO_{2(g)}$ lies very close to the partial pressure in the atmosphere (Godelitsas *et al*., 2003). In the same study, it was also argued that hydrocerussite formation might result from a rapid pH increment but that a subsequent equilibrium with the atmospheric $CO_{2(g)}$ can lead to a higher stability of cerussite. Our studies confirmed the fact that the formation of hydrocerussite was caused by the increment in the pH, but it revealed also that exchanging CO_2 with the atmosphere during a period of four hours did not lead to any conversion of hydrocerussite into cerussite. It must be stressed here that a time period of four hours is very short to be able to draw a sharp conclusion about the relative stability of cerussite/hydrocerussite within the solution medium as phase transitions might sometimes be kinetically controlled.

Moreover, the morphological stability of cerussite and hydrocerussite was tested for the dried samples that were kept under ambient conditions for a period of nine months. SEM and EDS analysis revealed that while hydrocerussite retained its morphologic configuration and chemical composition over this time period, a slow morphological transition was observed in the case of cerussite from columnar prismatic shape to what seems to be a rectangular plate-like shape. Figure 7(b) shows some cerussite crystals that are undergoing this morphological transition. The results were confirmed by duplicate samples prepared under identical conditions and stored under identical conditions (room temperature, atmospheric pressure). Similar analysis of the strontianite crystals showed that the needle-like morphology and chemical composition were retained over the same time period.

The atomic percentages of Pb, Sr, and Ca in the samples were determined using the EDS analysis. The results are given in Table 4. The data confirms again the enhanced dissolution of calcite—indicated by the increased deple-

tion in Ca content—upon overgrowth of hydrocerussite and strontianite. While the sorbed amounts of Pb^{2+} and Sr^{2+} seems to be not much affected by increasing the initial pH to 10.0 for the mixtures prepared at initial concentrations of 1.0×10^{-5} and 1.0×10^{-3} M, the amounts of scavenged ions upon precipitate formation is largely increased. In particular, the results indicate a very large removal of Pb compared to Sr, the thing that can be viewed better if the data is expressed on a mass percentage basis (~78% Pb and ~27% Sr, of the cation carbonate), which points to the higher efficiency of calcite in Pb removal from aqueous solutions.

DRIFT analysis of Sr-loaded calcite samples gave identical results as those obtained above for the mixtures prepared without any pH control except for showing a broadening in the in-plane-bending mode, $\nu4$, upon strontianite formation. The DRIFT spectra of Pb-reacted calcite are given in Fig. 7. The incorporation of Pb within the calcite structure is causing again various changes in the vibrational modes of carbonate. The changes observed for the samples prepared by reacting calcite with Pb^{2+} solutions having the initial concentrations of 1.0×10^{-5} and 1.0×10^{-3} M seems to be unaffected by the increase in the initial pH (an increase of about 1 pH unit). The DRIFT spectra of hydrocerussite, however, showed some differences from those of cerussite. As illustrated in Fig. 7(a), the band occurring at 3538 cm^{-1} is originating from the stretching vibrations of the structural—OH groups in hydrocerussite. As in cerussite, hydrocerussite formation caused a red shift of the band center to 1376 cm^{-1}. The band corresponding to the $\nu1$ mode (symmetric stretching that is IR inactive in calcite) became more distinct upon hydrocerussite overgrowth compared to the case of cerussite. Moreover, it is evident from the spectra that hydrocerussite formation weakened the $\nu2$ band (out-of-plane bending) and that the $\nu4$ band (in-plane bending) evolved at 676 cm^{-1} (compared to 712 cm^{-1} in calcite). As was previously discussed, the splits in the $\nu3$ and $\nu4$ modes and the activation of the $\nu1$ mode all point to geometrical modifications (point group variation) resulting in a decrease in the symmetry of the carbonate group upon the uptake of Pb^{2+} and Sr^{2+} ions by calcite even in the absence of a precipitate formation of these ions.

Conclusions

- Calcite is more effective in the removal of Pb^{2+} ions from aqueous solution compared to the removal of Sr^{2+} ions.
- At low aqueous concentrations (1.0×10^{-5} and 1.0×10^{-3} M), the sorption mechanism seems to proceed via incorporation of the sorbed ions within the interstitial positions or exchanging them for structural Ca^{2+}.

- When the initial concentration of Pb^{2+} and Sr^{2+} ions is raised to 0.10 M, a rapid overgrowth of strontianite and cerussite was observed. Increasing the initial pH to 10.0 caused enhancement in the dissolution of calcite, increase in the amount of precipitated strontianite and the formation of hydrocerussite instead of cerussite.
- The SEM images showed that the morphologies of strontianite, cerussite, and hydrocerussite have needle-like, columnar prismatic-like, and tabular hexagonal-like shapes, respectively. SEM and EDS analysis of the dry samples stored under ambient conditions for a period of nine months indicated that while hydrocerussite and strontianite retained their morphological structure and chemical composition, cerussite seemed to undergo a morphological transition yielding rectangular plate-like shape.
- The uptake of Pb^{2+} and Sr^{2+} results in decreasing the symmetry of the carbonate group (in calcite) as evident from the changes in various vibrational bands.

References

Abollino, O., Aceto, M., Malandrino, M., Sarzanini, C. and Mentasti, E. (2003) Adsorption of heavy metals on Na-montmorillonite. Effect of pH and organic substances. *Water Res.* **37**, 1619–1627.

Adhikari, T. and Singh, M. V. (2003) Sorption characteristics of lead and cadmium in some soils of India. *Geoderma* **114**, 81–92.

Axe, L., Tyson, T., Trivedi, P. and Morrison, T. (2000) Local structure analysis of strontium sorption to hydrous manganese oxide. *J. Colloid Interf. Sci.* **224**, 408–416.

Böttcher, M. E. (1997) Comment "Solid solution partitioning of Sr^{2+}, Ba^{2+}, and Cd^{2+} to calcite" by A. J. Tesoriero and J. F. Pankow. *Geochim. Cosmochim. Acta* **61**, 661–662.

Böttcher, M. E., Gehlken, P. and Steele, D. F. (1997) Characterization of inorganic and biogenic magnesian calcites by Fourier Transform infrared spectroscopy. *Solid State Ionics* **101–103**, 1379–1385.

Busenberg, E. and Plummer, L. N. (1985). Kinetics and thermodynamic factore controlling the distribution of SO_4^{2-} and Na^+ in calcites and selected aragonites. *Geochim. Cosmochim. Acta* **49**, 713–725.

Cherniak, D. J. (1997) An experimental study of strontium and lead diffusion in calcite, and implications for carbonate diagenesis and metamorphism. *Geochim. Cosmochim. Acta* **61**, 4173–4179.

Curti, E. (1999) Coprecipitation of radionuclides with calcite: estimation of partition coefficients based on a review of laboratory investigations and geochemical data. *Applied*

Geochem. **14**, 433–445.

Godelitsas, A., Astilleros, J. M., Hallam, K., Harissopoulos, S. and Putnis, A. (2003) Interaction of calcium carbonates with lead in aqueous solutions. *Environment. Sci. Techn.* **37**, 3351–3360.

Hay, M. B., Workman, R. K. and Manne, S. (2003) Mechanisms of metal ion sorption on calcite: composition mapping by Lateral Force Microscopy. *Langmuir* **19**, 3727–3740.

Hooda, P. S. and Alloway, B. J. (1998) Cadmium and lead sorption behaviour of selected English and Indian soils. *Geoderma* **84**, 121–134.

Kuriyavar, S. I., Vetrivel, R., Hegde, S. G., Ramaswamy, A. V., Chakrabarty, D. and Mahapatra, S. (2000) Insights into the formation of hydroxyl ions in calcium carbonate: temperature dependent FTIR and molecular modelling studies. *J. Mater. Chem.* **10**, 1835–1840.

Lieser, K. H. (1995) Radionuclides in the geosphere: sources, mobility, reactions in natural waters and interactions with solids. *Radiochim. Acta* **70/71**, 355–375.

Lin, Z., Comet, B., Qvarfort, U. and Herbert, R. (1995) The Chemical and mineralogical behaviour of Pb in shooting range soils from central Sweden. *Environ. Pollut.* **89**, 303–309.

Marani, D., Macchi, G. and Pagano, M. (1995) Lead precipitation in the presence of sulphate and carbonate: testing of thermodynamic predictions. *Water Res.* **29**, 1085–1092.

Morse, J. W. (1986) The surface chemistry of calcium carbonate minerals in natural waters: An overview. *Mar. Chem.* **20**, 91–112.

Nakamoto, K. (1986) *Infrared and Raman Spectra of Inorganic and Coordination Compounds*. John Wiley & Sons, pp. 86–87.

O'Reilly, S. E. and Hochella, M. F., Jr. (2003) Lead sorption efficiencies of natural and synthetic Mn and Fe-oxides. *Geochim. Cosmochim. Acta* **67**, 4471–4487.

Parkman, R. H., Charnock, J. M., Livens, F. R. and Vaughan D. J. (1998) A study of the interaction of strontium ions in aqueous solution with the surfaces of calcite and kaolinite. *Geochim. Cosmochim. Acta* **62**, 1481–1492.

Pingitore, N. E., Jr., Lytle, F. W., Davies, B. M., Eastman, M. P., Eller, P. G. and Larson, E. M. (1992) Mode of incorporation of Sr^{2+} in calcite: Determination by X-ray absorption spectroscopy. *Geochim. Cosmochim. Acta* **56**, 1531–1538.

Ponizovsky, A. A. and Tsadilas, C. D. (2003) Lead(II) retention by Alfisol and clinoptilolite: cation balance and pH effect. *Geoderma* **115**, 303–312.

Reig, F. B., Gimeno Adelantado, J. V. and Moya Moreno, M. C. M. (2002) FTIR quantitative analysis of calcium carbonate (calcite) and silica (quartz) mixtures using the constant ratio method. Application to geological samples. *Talanta* **58**, 811–821.

Sahai, N., Carroll, S. A., Roberts, S. and O'Day, P. A. (2000) X-ray absorption spectroscopy of strontium(II) coordination: II. sorption and precipitation at kaolinite, amorphous silica, and goethite surfaces. *J. Colloid Interf. Sci.* **222**, 198–212

Schosseler, P. M., Wehrli, B. and Schweiger, A. (1999) Uptake of Cu^{2+} by the calcium carbonates vaterite and calcite as studied by continuous wave (cw) and pulse electron paramagnetic resonance. *Geochim. Cosmochim. Acta* **63**, 1955–1967.

Skoog, D. A., West, D. M. and Holler, F. J. (1996) *Analytical Chemistry*. 7th ed., Saunders College Publishers, App. 2, pp. A-6.

Sturchio, N. C., Chiarello, R. P., Cheng, L., Lyman, P. F., Bedzyk, M. J., Qian, Y., You, H., Yee, D., Geissbuhler, P., Sorensen L. B., Liang, Y. and Baer, D. R. (1997) Lead adsorption at the calcite-water interface: Synchrotron X-ray standing wave and X-ray reflectivity studies. *Geochim. Cosmochim. Acta* **61**, 251–263.

Sverjensky, D. A. and Molling, P. A. (1992) A linear free energy relationship for crystalline solids and aqueous ions. *Nature* **356**, 231–234.

Zachara, J. M., Cowan, C. E. and Resch, C. T. (1991) Sorption of divalent metals on calcite. *Geochim. Cosmochim. Acta* **55**, 1549–1562.